Journal of Catalysis 272 (2010) 74–81

Contents lists available at ScienceDirect

Journal of Catalysis

journal homepage: www.elsevier.com/locate/jcat

Mechanism and site requirements for NO oxidation on Pd catalysts

Brian M. Weiss, Enrique Iglesia *

Department of Chemical Engineering, University of California at Berkeley, Berkeley, CA 94720, United States

ARTICLE INFO

Article history:
Received 8 January 2010
Revised 22 February 2010
Accepted 7 March 2010
Available online 9 April 2010

Keywords:
NO_x storage
Oxidation catalysis
Nitric oxide
Palladium
Lean NO_x traps
Cluster size effects

ABSTRACT

Kinetic and isotopic methods were used to establish the identity and kinetic relevance of elementary steps and the effects of cluster size for NO oxidation on supported Pd catalysts. O_2 activation on vacancies within nearly saturated oxygen adlayers is the sole kinetically relevant step. Water, present in combustion effluents, inhibits NO oxidation via reversible adsorption on vacancies to form unreactive OH species. The coverage and chemical potential of oxygen are determined by the NO_2/NO ratios prevalent during catalysis; they are rigorously described by O_2 virtual pressures accessible to measurement. At a given oxygen chemical potential, O_2 activation during $^{16}O_2$–$^{18}O_2$ exchange and NO oxidation occurs at similar rates, indicating that NO-assisted O_2 activation is not required for NO oxidation turnovers. These findings confirm the rigor and relevance of O_2 virtual pressure as a measurable surrogate for the oxygen chemical potential during catalysis, as well as the role of mobile oxygen species, which allow O_2 dissociation to occur on isolated vacancies. Oxygen chemical potentials prevalent during NO oxidation cause active clusters to exist as PdO at all relevant conditions, consistent with steady-state turnover rates that are insensitive to reductive or oxidative treatments. NO oxidation turnover rates decrease as PdO clusters become smaller because of stronger oxygen binding and lower vacancy concentrations in small clusters. The catalytic consequences of size are similar on PdO and Pt clusters, despite their different oxidation state, consistent with a common requirement for surface vacancies in O_2 activation steps on both catalysts. Such requirements lead to strong NO_2 inhibition effects and to a marked increase in NO oxidation rates when NO_2 adsorbents, present as physical mixtures, decrease NO_2 concentrations near active sites.

1. Introduction

Combustion engines become more efficient at high air-to-fuel ratios, but these conditions lead to higher NO_x levels and low reductant (CO, hydrocarbons) concentrations in effluent streams [1]. Conventional exhaust catalysts are ineffective for these systems; an alternate abatement strategy first oxidizes NO to NO_2, which then adsorbs on metal oxides [2]. NO oxidation is also critical in soot combustion, in which NO_2 acts as an oxygen carrier between carbon particles and non-vicinal metal clusters that dissociate O_2 [3]. Pt is often used to catalyze NO oxidation, but Pd [4–7] and other transition metals [8–11] also show significant reactivity. The mechanism and site requirements for NO oxidation on Pd catalysts have not been addressed in previous studies [12], and rigorous mechanistic and reactivity comparisons between Pd and Pt catalysts have not been reported to date.

O_2 interacts with sparse vacancies on surfaces nearly saturated with chemisorbed oxygen (O^*) in the kinetically relevant step for NO oxidation on supported Pt clusters [13,14]. O^* coverages reflect the equilibration of NO and NO_2 with surface vacancies [13,14]. A comparison between the rates of isotopic oxygen exchange and NO oxidation confirmed the kinetic significance of O_2 activation steps and suggested that O_2 dissociation involves mobile oxygen-derived intermediates [14]. NO oxidation and oxygen exchange rates decreased sharply with decreasing Pt cluster size [14,15] because O^* binds more strongly on the coordinatively unsaturated Pt atoms that prevail on small cluster surfaces [14]. NO oxidation catalysis on Pt is inhibited by NO_2 because of its role in establishing O^* coverages during steady-state NO oxidation catalysis; as a result, NO oxidation rates are much higher when Pt catalysts are mixed with NO_2 adsorbents, because they decrease local NO_2 concentrations at active sites [14].

Here, we provide evidence for the elementary steps and cluster size effects in NO oxidation catalyzed by PdO. Kinetic and isotopic methods show that rate-determining steps are similar on Pd and Pt catalysts, but that Pd clusters are present as oxides during NO oxidation, in contrast to Pt clusters, which retain their metallic bulk character. Water, a ubiquitous component in automotive exhaust, inhibits NO oxidation by forming hydroxyls on vacant sites (*) required in kinetically relevant steps. NO oxidation rates are significantly higher on larger PdO clusters, a trend also observed on Pt clusters [14,15]; these trends reflect the stronger oxygen bonds on the surfaces of smaller clusters, which lead to lower vacancy

* Corresponding author. Fax: +1 510 642 4778.
E-mail addresses: iglesia@berkeley.edu, iglesia@cchem.berkeley.edu (E. Iglesia).

0021-9517/$ - see front matter © 2010 Elsevier Inc. All rights reserved.
doi:10.1016/j.jcat.2010.03.010

concentrations. We show that NO oxidation rates are significantly higher in intimate mixtures of Pd catalysts and $BaCO_3$ adsorbents, which scavenge NO_2 and decrease NO_2 local concentrations and its inhibiting effect on NO oxidation, thus confirming the critical synergy between the metal and adsorbent functions in lean NO_x traps.

2. Experimental methods

2.1. Material synthesis and catalyst characterization

γ-Al_2O_3 (Sasol, SBa-200) supports were heated at 0.07 K s^{-1} to 1023 K in flowing dry air (Praxair, Extra Dry, 1 cm^3 s^{-1} g^{-1}) and held for 4 h. A 10 wt.% $Pd(NH_3)_4(NO_3)_2$ aqueous solution (Sigma–Aldrich, 99.99% metal purity) diluted with de-ionized distilled water (Barnstead, Nanopure) was added dropwise to γ-Al_2O_3 to the incipient wetness point (0.45 g solution (g $Al_2O_3)^{-1}$) to prepare catalyst samples with 1.0 and 1.5 wt.% Pd contents. Impregnated supports were treated in ambient air to 393 K for 4 h and then in 9% H_2/He (Praxair, 99.999% purity, 1 cm^3 s^{-1} g^{-1}) for 4 h by heating at 0.07 K s^{-1} to a temperature between 773 and 1023 K. Samples were subsequently treated in He (Praxair, 99.999% purity, 1 cm^3 s^{-1} g^{-1}) at 773 K for 1 h and then in 0.5% O_2/He (Praxair, 99.999% purity, 1 cm^3 s^{-1} g^{-1}) at ambient temperature for 1 h to passivate their surfaces. Adsorbents (15 wt.% $BaCO_3/Al_2O_3$) were prepared from $Ba(O_2C_2H_3)_2$ (Sigma–Aldrich, 99.995%) precursors by incipient wetness methods described previously [14].

The fraction of surface Pd atoms (Pd_s) was measured by O_2 chemisorption using an Autosorb-1 titration apparatus (Quantachrome). Catalysts (1 g) were treated at 673 K (0.07 K s^{-1} heating rate) in flowing H_2 (Praxair, 99.999%, 0.2 cm^3 s^{-1} g^{-1}) for 1 h and then under vacuum for 1 h. Pd dispersions were determined from irreversible O_2 (Praxair, 99.993%) uptakes at 313 K assuming a stoichiometry of one O-atom per surface Pd atom [16]. Average cluster diameters were estimated from dispersion values, by assuming spherical clusters with atomic densities for bulk Pd metal (12 g cm^{-3}; 68 Pd nm^{-3}) [17]. These procedures gave samples with 0.08–0.74 Pd dispersions and 1–10 nm average cluster diameters.

2.2. NO oxidation rate measurements

NO oxidation rates were measured on pre-formed pellets (0.12–0.18 mm) of Pd/Al_2O_3 catalysts and on mixtures of Pd/Al_2O_3 and $BaCO_3/Al_2O_3$ that were combined within pellets (0.12–0.18 mm) or as intrapellet mixtures (0.12–0.18 mm to 0.18–0.25 mm). Samples were held on a porous quartz (10 mm) frit within a tubular flow reactor (10 mm). Reactant (15% O_2/He, 2% NO/He, 1% NO_2/He, and 5% CO_2/He) and He carrier gases (Praxair, 99.999% purity) were metered by electronic controllers (Porter Instruments) and their relative flows varied to achieve a range of reactant pressures (1–12 kPa O_2, 0.04–0.25 kPa NO, 0.02–0.25 kPa NO_2, 0–2 kPa CO_2). A syringe pump (Cole Parmer, 74900 series) introduced H_2O (0.001–1 kPa) from a 0.5-cm^3 syringe (Hamilton) into lines held at 340 K and swept by the reactant stream. A resistively heated furnace with a feedback controller (Watlow, 96 series) and a K-type thermocouple maintained catalyst temperatures between 553 and 698 K. The concentrations in the inlet and outlet streams were measured by an infrared analyzer (MKS 2030; 2 cm^3 cell; 2 cm path length; 338 K). NO oxidation rates are reported as turnover rates (moles NO converted (mol $Pd_s)^{-1}$ s^{-1}) at NO conversions below 20% and calculated using design equations for plug-flow reactors. Heat and mass transfer artifacts were ruled out by dilution experiments using the Koros–Nowak criteria [18]. For each experiment, the independent variable was changed randomly, while catalyst stability was verified by repeating conditions. NO oxidation measurements on catalysts and catalyst–adsorbent mixtures were preceded by treatments in 5 kPa O_2/He and 5 kPa O_2/0.5 kPa CO_2/He, respectively, at temperatures between 573 and 698 K for 1 h.

2.3. Isotopic oxygen exchange rate measurements

$^{16}O_2$–$^{18}O_2$ exchange rates were measured in a gradientless batch reactor (498 cm^3 volume) that was re-circulated by a graphite gear pump (Micropump; 2 cm^3 s^{-1}). Gases (99.999% chemical purity) were obtained from Praxair (90% O_2/Ar, He) and Ikon Isotopes ($^{18}O_2$, 96% isotopic ^{18}O purity). Catalysts were heated to reaction temperature (643–698 K) at 0.07 K s^{-1} and held for 1 h in flowing 2 kPa $^{16}O_2$/Ar/He (30 cm^3 s^{-1} g^{-1}) before the reactor was evacuated and filled with an equimolar $^{16}O_2$–$^{18}O_2$ mixture and He as balance. Isotopomer concentrations during $^{16}O_2$–$^{18}O_2$ exchange were measured by periodic injections into a mass spectrometer (Spectra Mini-Lab).

The exchange rates of $^{18}O_2$(g) with pre-adsorbed $^{16}O^*$ were measured in the tubular flow reactor described in Section 2.2 with isotopic analysis by a mass spectrometer (Spectra Mini-Lab). Pre-reduced catalysts were heated from ambient temperature to 698 K at 0.08 K s^{-1} in flowing 2 kPa $^{16}O_2$ (1 cm^3 s^{-1} g^{-1}) and held for 1 h to form PdO [19,20]. $^{18}O_2$–$^{16}O^*$ exchange rates were measured in flowing 2 kPa $^{18}O_2$/He (Ikon Isotopes, 96% atom purity; 1 cm^3 s^{-1} g^{-1}) isothermally (698 K) or during a temperature ramp from 373 to 773 K (0.17 K s^{-1}).

3. Results and discussion

3.1. NO oxidation kinetics and elementary steps on Pd catalysts

The effects of NO, NO_2, and O_2 pressure on NO oxidation rates are shown in Fig. 1 for one of the Pd/Al_2O_3 catalysts used in this study (0.33 Pd dispersion). Forward NO oxidation rates ($\vec{r}_{NO}$) were derived from measured rates (r_{NO}) by accounting for the approach-to-equilibrium [21] of NO oxidation reactions:

$$2NO + O_2 \rightleftarrows 2NO_2 \quad (1)$$

$$r_{NO} = \vec{r}_{NO}(1 - \eta) \quad (2)$$

$$\eta = [NO_2]^2[NO]^{-2}[O_2]^{-1}K_R^{-1} \quad (3)$$

where K_R is the known equilibrium constant [17] for the overall reaction defined by Eq. (1).

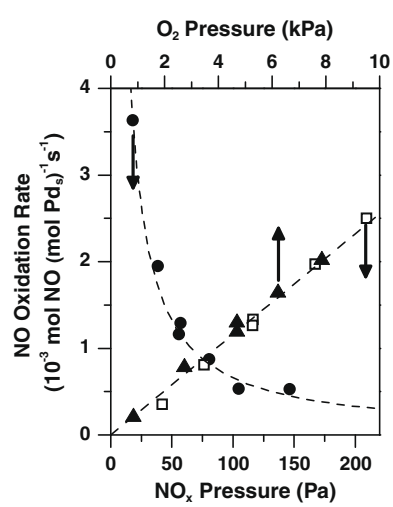

Fig. 1. The NO oxidation rate on Pd/Al_2O_3 (0.33 dispersion) at 603 K versus NO_2 (●), NO (□), and O_2 (▲). Each pressure was varied independently while the others were held constant at 5 kPa O_2, 0.056 kPa NO_2, and 0.112 kPa NO.

Steady-state forward NO oxidation rates were accurately described by the equation:

$$\vec{r}_{NO} = k_{app}[O_2][NO][NO_2]^{-1} \quad (4)$$

as shown by the dashed lines in Fig. 1. This rate equation is the same as that found for NO oxidation on Pt metal clusters [13,14], suggesting that kinetically relevant steps are the same on both catalysts. We conclude that NO oxidation on Pd also involves kinetically relevant O_2 reactions on isolated vacancies (*) within a nearly saturated O* adlayer (Step 1, Scheme 1) [13,14]. Vacancy concentrations are determined by the equilibration of NO, NO_2, and O* (Step 2, Scheme 1). The subsequent O_2 dissociation steps are not accessible to measurement during steady-state catalysis and are represented by the ellipsis shown in Scheme 1. The elementary steps in Scheme 1 are consistent with the approach-to-equilibrium factor in Eq. (3) and with the rate expression of:

$$\vec{r}_{NO} = \frac{2k_1[O_2]}{1 + K_2[NO_2][NO]^{-1}} \quad (5)$$

when * and O* are the most abundant surface intermediates. This expression simplifies to Eq. (4), which describes all measured rate data on Pd, when $(*) \ll (O^*)$.

The * and O* surface coverages and the tendency of Pd clusters to form bulk oxides depend on the oxygen chemical potential at catalyst surfaces. This oxygen chemical potential can be expressed as a virtual oxygen pressure, O_2^v [14,21], defined as the O_2 pressure that would give at conditions of adsorption–desorption equilibrium the same O* coverage present during steady-state catalysis in the presence of a given NO–NO_2 mixture. The equilibrium reaction that determines O* during steady-state NO oxidation (Step 2, Scheme 1) is equivalent to the combined Steps 2a and 2b (Scheme 1), which give the value of O_2^v as:

$$[O_2^v] = [NO_2]^2[NO]^{-2}K_R^{-1} \quad (6)$$

where K_R is the known equilibrium constant [17] for the overall NO oxidation reaction (Eq. (1)). This treatment shows that K_2, the equilibrium constant for the interaction of NO and O*, is related to the equilibrium constant for O_2 adsorption, K_O:

$$K_2 = K_O^{1/2}/K_R^{1/2} \quad (7)$$

The forward NO oxidation rate expression depends only on the prevalent O_2(g) pressure and the virtual oxygen pressure (O_2^v) as shown by combining Eqs. (5)–(7):

$$\vec{r}_{NO} = \frac{2k_1[O_2(g)]}{1 + (K_O[O_2^v])^{1/2}} \quad (8)$$

This expression shows that the effective NO oxidation rate constant depends only on the rate constant for O_2 activation on isolated vacancies (k_1) and on the standard thermodynamic properties of atomic O* species (K_O) on nearly saturated surfaces.

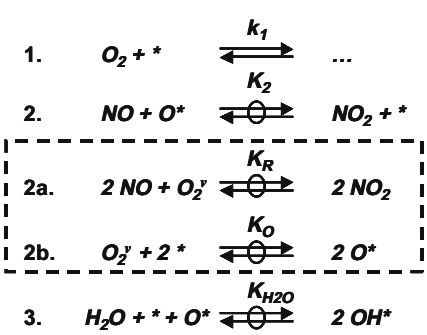

Scheme 1. Proposed elementary NO oxidation steps.

NO oxidation occurs sufficiently near thermodynamic equilibrium (η values of 0.01–0.30) for its reverse reaction (NO_2 decomposition) to occur at detectable rates. The rate of this reverse reaction is obtained from the forward rate (Eq. (8)) and the approach-to-equilibrium factor, η (Eq. (3)):

$$\overleftarrow{r}_{NO} = \frac{2k_1[O_2^v]}{1 + (K_O[O_2^v])^{1/2}} \quad (9)$$

Eq. (9) is consistent with the thermodynamics for the overall reaction, for which forward and reverse NO oxidation rates become identical at chemical equilibrium when the oxygen chemical potential at the surface, O_2^v, and in the gas phase, O_2(g) are equal.

3.2. Isotopic oxygen exchange and NO oxidation rates

We probe next the kinetic relevance and reversibility of the proposed O_2 activation step by considering the mechanism and rates of oxygen isotopic exchange, a reaction that reflects the dynamics and thermodynamics of the interaction between O_2 and catalyst surfaces. A rigorous comparison of exchange and NO oxidation rates first requires an interpretation of isotopic exchange measurements in terms of O_2 activation rates, which we derive briefly by following previous methods [14,22].

$^{16}O_2$–$^{18}O_2$ exchange in the absence of co-reactants occurs at chemical equilibrium, while reaction intermediates are present at their pseudo-steady-state concentrations. Thus, the overall desorption rate of O_2 from the surface equals the O_2 adsorption rate (r_{O_2}), and the net reaction rate of each O_2 isotopomer is equal to the observed exchange rate (r_{ex}):

$$r_{O_2} = \sum \vec{r}_{ik} = \sum \overleftarrow{r}_{ik} \quad (10)$$

$$r_{ex} = (\vec{r}_{ik} - \overleftarrow{r}_{ik})/\nu_{ik} \quad (11)$$

where i and k denote each oxygen isotope (^{16}O or ^{18}O) and the stoichiometric factors (ν_{ik}) are for the overall exchange reaction:

$$^{18}O_2 + {}^{18}O_2 \rightleftarrows 2\,{}^{16}O^{18}O \quad (12)$$

Eqs. (10) and (11) give solutions for the reaction rates of each O_2 isotopomer:

$$\vec{r}_{ik} = r_{O_2}y_{ik} \quad (13)$$

$$\overleftarrow{r}_{ik} = |\nu_{ik}|r_{O_2}x_ix_k \quad (14)$$

where x_i and x_k are the fractions of each isotope in the reaction mixture and y_{ik} is the fraction of each [$^iO^kO$] isotopomer among O_2 molecules. The exchange rate (r_{ex}) then is related to r_{O_2} by:

$$\frac{r_{ex}}{y_{^{16}O_2}y_{^{18}O_2}} = r_{O_2}(1 - \eta_{ex}) \quad (15)$$

$$\eta_{ex} = \frac{y_{^{16}O^{18}O^2}}{4y_{^{16}O_2}y_{^{18}O_2}} \quad (16)$$

The denominator term in Eq. (15) reflects the probability that a reaction event increases the $^{16}O^{18}O$ content, and η_{ex} accounts for the approach of the system to isotopic equilibrium.

The relationship between exchange rates (r_{ex}) and O_2 activation rates (r_{O_2}) in Eq. (15) allows $^{16}O_2$–$^{18}O_2$ exchange rates to be compared rigorously with NO oxidation rates. Specifically, we compare O_2 activation rates during exchange (r_{O_2}) and NO oxidation ($r_{NO}/2$) at a particular value of the surface and gas phase oxygen chemical potentials (2 kPa $O_2^{(v,g)}$; Fig. 2). NO oxidation rates were measured near chemical equilibrium at 2 kPa O_2^v and either 0 or 7 kPa O_2(g), and corrected to their equilibrium values (at 2 kPa O_2^v, 2 kPa O_2(g)) by Eqs. (8) and (9). The $^{16}O_2$–$^{18}O_2$ exchange rates are

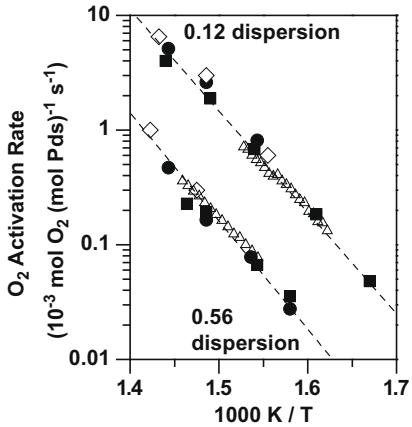

Fig. 2. Arrhenius plots from Pd/Al_2O_3 (0.12 and 0.56 dispersion) of rates extrapolated to 2 kPa $O_2^{v,g)}$ for (■) NO oxidation (2 kPa O_2^v, 7 kPa O_2(g)); (●) NO_2 decomposition (2 kPa O_2^v; 0 kPa O_2(g)); (△) $^{16}O_2$–$^{18}O_2$ exchange (2 kPa O_2(g)); and (◇) $^{18}O_2$–$^{16}O^*$ exchange (2 kPa O_2(g)) for uptakes less than 0.1 ^{18}O $(Pd_s)^{-1}$.

the same as those for NO oxidation between 643 and 698 K with apparent activation energies for both reactions of 148 and 152 kJ mol^{-1} on 0.12 and 0.56 dispersion Pd/Al_2O_3 catalysts, respectively. The similar rates of exchange and NO oxidation are consistent with their common kinetically relevant steps on both high and low dispersion Pd/Al_2O_3 and with the reversibility of the O_2 dissociation steps by the microscopic reverse of the forward reaction. When exchange occurs via the steps in Scheme 1, the reaction rate of each O_2 isotopomer equals the difference between the forward and reverse rates for Step 1:

$$r_{ik} = k_1[{}^iO^kO][*] - \overleftarrow{r}_{ik} \tag{17}$$

Vacancies are present at concentrations given by their virtual equilibrium with O_2^v during NO oxidation and by their actual equilibrium with O_2(g) during exchange. The rate of O_2 activation events during exchange is then described by:

$$r_{O_2} = \frac{k_1[O_2]}{1 + (K_O[O_2])^{1/2}} \tag{18}$$

This expression is identical to those for the forward and reverse NO oxidation rates (Eqs. (8) and (9)) when O_2(g) and O_2^v are equal during exchange and NO oxidation, respectively. $^{16}O_2$–$^{18}O_2$ exchange rates (at 673 K) increased from 0.004 to 0.015 mol O_2 (mol $Pd_s)^{-1}$ s^{-1} as the O_2 pressure increased from 2 kPa O_2 to 20 kPa, consistent with an oxygen dependence of $[O_2]^{0.5}$. The rates and mechanisms of isotopic exchange and NO oxidation are also similar to each other on Pt [14], consistent with the rigorous description of the O^* chemical potential by O_2^v and with identical rate-determining steps involving isolated vacancies within O^*-saturated layers on both Pt and Pd catalysts. Indeed, both NO oxidation [4–10,13,14] and O_2 exchange [14,23] and also NO decomposition [24] and O_2 reduction in fuel cell applications [25] are efficiently catalyzed by similar transition metals (e.g. Pt, Pd, CoO_x) suggesting mechanistic similarities in the oxygen dissociation and recombination steps during all of these reactions.

A kinetically relevant step involving a single vacancy and O_2(g), which is a weakly bound, molecular precursor to O^* adatoms [26,27], requires significant mobility of either vacancies or superoxo-species for O_2^* to dissociate before desorbing. Previous computational results have suggested that NO bound on sites adjacent to chemisorbed O_2^* may be involved in dissociation and relevant to measured NO oxidation rates [28], but O_2 dissociation actually occurs as fast in the absence of NO, indicating that alternate pathways not requiring NO^* are involved.

We probe the mobility of these surface intermediates involved in O_2 dissociation by considering isotopomer selectivities during transient exchange of $^{18}O_2$ with pre-adsorbed $^{16}O^*$ on Pd/Al_2O_3. Initial $^{18}O_2$–$^{16}O^*$ exchange rates were identical to both $^{16}O_2$–$^{18}O_2$ exchange and NO oxidation rates on Pd/Al_2O_3 samples with both high and low dispersion (Fig. 2). $^{18}O_2$ conversion rates during $^{18}O_2$–$^{16}O^*$ exchange reflect the same kinetically relevant step during $^{16}O_2$–$^{18}O_2$ exchange and NO oxidation (Step 1 in Scheme 1; Eq. (17)). Both $^{16}O^{18}O$ and $^{16}O_2$ formed as initial products of isothermal $^{18}O_2$–$^{16}O^*$ exchange with their selectivities given in Table 1 for large and small Pd clusters. Similar non-zero initial selectivities to $^{16}O^{18}O$ were observed during previous measurements of isothermal $^{18}O_2$–$^{16}O^*$ exchange on PdO [29] and during temperature program $^{18}O_2$–$^{16}O^*$ exchange on Pt catalysts [14]. The initial formation of $^{16}O^{18}O$ and the kinetic relevance of O_2 dissociation on isolated vacancies for exchange events are consistent with dissociation steps occurring on *–O^* site pairs to give mobile superoxo-intermediates (Scheme 2, Step 1), with the same rate constant as Step 1 in Scheme 1 (k_1). This intermediate then reacts with a vicinal O^* during migration and desorbs with another O^* (to form $^{16}O^{18}O$ in the early stages of exchange when $^{16}O^*$ is the most abundant surface isotopomer) or combines with a distant vacant site to form a strongly chemisorbed O^* species (Scheme 2, Step 1a). The initial selectivity to $^{16}O_2$ during $^{18}O_2$–$^{16}O^*$ exchange arises from $^{16}O^*$ that has been mobilized to a superoxo-position, rather than by the direct recombination of vicinal $^{16}O^*$ species. The elementary steps in Scheme 2 give an expression for the initial isotopomer selectivity during $^{18}O_2$–$^{16}O^*$ exchange in terms of the ratio of the rates of each step in Scheme 2:

$$\left.\frac{\overleftarrow{r}_{^{16}O^{18}O}}{\overleftarrow{r}_{^{16}O_2}}\right|_{t=0} = \frac{r_{O_2}}{k_{-1a}} \tag{19}$$

Our results indicate that mobile oxygen species form at similar rates by O_2 adsorption and O^* mobilization, apparently because both steps depend directly on the strength of surface oxygen bonds. Small clusters give much smaller exchange rates and higher initial selectivities to $^{16}O^{18}O$. These trends reflect in both cases stronger O^* bonds on smaller clusters (as we discuss in Section 3.4), which lead in turn to smaller vacancy concentrations and to less frequent

Table 1
Rates and selectivities of $^{18}O_2$ exchange with pre-adsorbed $^{16}O^*$.

Catalyst dispersion[a]	Initial $^{18}O_2$ conversion rate[b] (10^{-3} mol $^{18}O_2$ (mol $Pd_s)^{-1}$ s^{-1})	Initial selectivity[b] ($^{16}O^{18}O/^{16}O_2$)
0.12	3.8	1.0
0.56	0.45	0.5

[a] 1.6 wt.% Pd/Al_2O_3.
[b] 698 K, 2 kPa $^{18}O_2$/He.

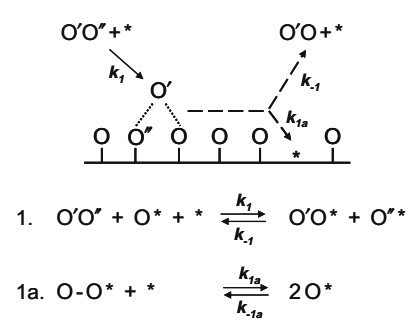

Scheme 2. O_2 dissociation elementary steps*. *: O, O′, and O″ denote different oxygen atoms involved in elementary reactions.

dissociation of superoxo-species on vacant sites. Mobile oxygen species have been previously proposed to account for O_2 formation on O^*-covered surfaces during NO decomposition on Pt at temperatures (573–698 K) similar to those required for the reverse of NO oxidation [24]. As expected, microscopic reversibility would implicate similar steps and the involvement of mobile oxygen species as intermediates in O_2 adsorption on metal surfaces nearly saturated with O^*.

3.3. Effect of H_2O and CO_2 pressures on NO oxidation rates

Combustion effluent streams contain significant levels of H_2O and CO_2. As a result, NO oxidation catalysts must function without strong inhibition by these combustion products. NO oxidation rates on Pd/Al_2O_3 (0.12 dispersion) were essentially unaffected by CO_2, but inhibited by H_2O (Fig. 3a). NO oxidation rates decreased with increasing NO_2/NO ratios at high H_2O pressures (Fig. 3b). These kinetic effects are accurately described by the equation:

$$\vec{r}_{NO} = \frac{2k_1[O_2]}{K_2[NO_2][NO]^{-1} + K_{app}[H_2O]^{1/2}[NO_2]^{1/2}[NO]^{-1/2}} \quad (20)$$

as shown by the dashed curves in Fig. 3a and b. The first term in denominator can be extracted to give:

$$\vec{r}_{NO} = \frac{r_O}{1 + K'_{app}[H_2O]^{1/2}[NO]^{1/2}[NO_2]^{-1/2}} \quad (21)$$

where r_o is the NO oxidation rate in the absence of H_2O (Eq. (4)). These H_2O inhibition effects reflect competitive reactions of H_2O and O_2 with O^*–* site pairs, in which H_2O forms unreactive OH species (Scheme 1, Step 4) that occupy vacant sites required for O_2 activation. Eq. (21) is equivalent to:

$$\vec{r}_{NO} = \frac{r_O}{1 + K_{H_2O}^{1/2}K_O^{-1/4}[H_2O]^{1/2}[O_2^v]^{-1/4}} \quad (22)$$

This equation applies for surfaces predominantly covered by O^* and OH^*; the second denominator term in Eqs. (21) and (22) represents the $(OH^*)/(O^*)$ ratio during steady-state NO oxidation catalysis. Similar inhibition and elementary steps involving H_2O have been reported for CH_4 and dimethylether oxidation on Pd catalysts [30,31], but inhibition effects were not detected for NO oxidation on Pt above 573 K [32], apparently because hydroxyls on Pt surfaces are less stable relative to chemisorbed oxygen than on PdO surfaces.

3.4. Site requirements and cluster size effects for NO oxidation on Pd catalysts

Next, we consider the catalyst oxidation state and cluster size and their consequences for NO oxidation turnover rates. The rigorous definition of an oxygen virtual pressure (Eq. (6)) allows the oxidation state of Pd clusters during steady-state catalysis to be determined purely from thermodynamic data.

We first confirmed that steady-state was achieved after both O_2 and H_2 treatments intended to form Pd oxide or metal clusters, respectively, on catalyst samples containing large clusters (0.12 dispersion; Fig. 4). NO conversion rates (at 0.17 kPa O_2^v, 5 kPa O_2, 603 K) were independent of initial treatment in H_2 (101 kPa, 2 h) or O_2 (101 kPa, 24 h) and reached constant values in both cases after ~3 h in contact with reactants. The formation of nitrates on Al_2O_3 from NO_2 in the inlet stream influenced initial NO conversion rates after both H_2 and O_2 treatments. The similar NO oxidation rates after H_2 or O_2 treatments indicate that Pd clusters formed identical structures during catalysis, irrespective of their initial state after pre-treatment. The thermodynamics of Pd/PdO transitions for bulk systems ($\Delta H_f^o = -119$ kJ mol^{-1}, $\Delta S_f^o = -109$ J mol^{-1} K^{-1} [33,34]) shows that PdO is the stable bulk phase at 603 K for

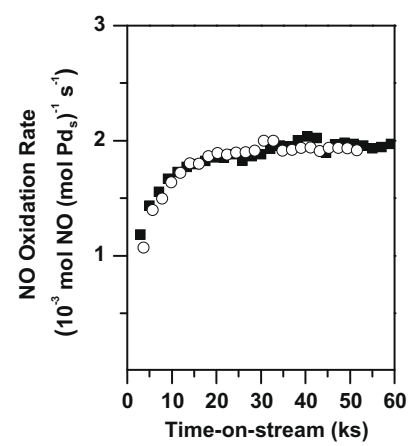

Fig. 4. NO oxidation rates on Pd/Al_2O_3 (0.12 dispersion) at 603 K, 0.17 kPa O_2^v, 5 kPa O_2 versus time-on-stream after catalyst treatment in 101 kPa H_2, 2 h, 603 K (○) and 15 kPa O_2, 24 h, 603 K (■).

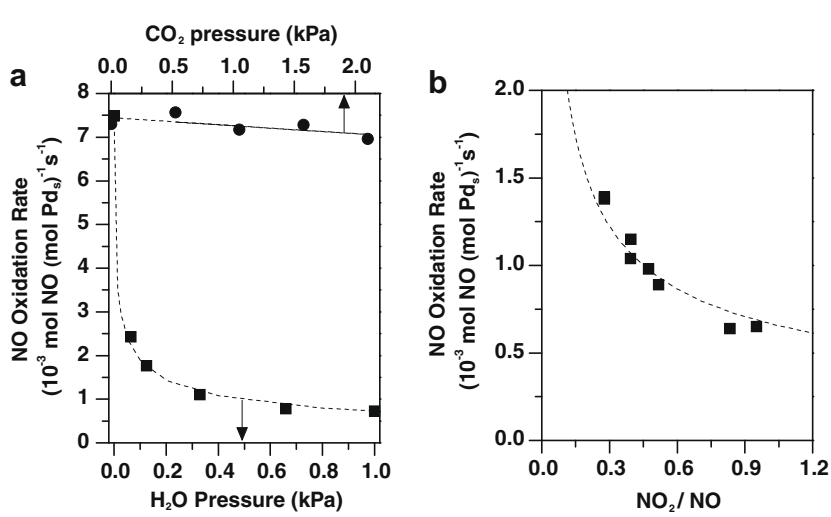

Fig. 3. The NO oxidation rate on Pd/Al_2O_3 (0.12 dispersion) at 648 K, (a) while H_2O (■) and CO_2 (●) were varied (8 kPa O_2, 0.050 kPa NO_2, and 0.14 kPa NO) and (b) while the NO_2/NO ratio was varied (12 kPa O_2, 1.25×10^{-3} kPa H_2O).

any oxygen chemical potentials corresponding to (virtual) O_2 pressures above 10^{-7} kPa. Pd(1 1 1) samples exposed to O_2 (6.5 kPa, 600 K) "adsorbed" ~20 O-atoms per surface Pd atom within 600 s, consistent with the formation of ~20 layers of a stable Pd oxide [35]. Thus, oxygen diffusion within the Pd bulk occurs sufficiently fast at typical NO oxidation temperatures to rapidly and completely oxidize Pd clusters smaller than ~10 nm.

NO oxidation rate constants (from rate data, Eq. (8), and η, Eq. (3)) were unaffected by O_2^{ν} pressures between 0.003 and 33 kPa at 623 K (Fig. 5); O_2^{ν} rigorously represents the kinetic and thermodynamic driving force for the oxidation of Pd clusters. Fig. 5 shows that Eq. (8) is valid and that $k_1K_O^{-1/2}$ values remain constant throughout this range of oxygen chemical potentials, implying that no changes in phase or structure consequential for reactivity occur throughout the range of NO oxidation conditions. Thus, catalytic clusters are either Pd metal or Pd oxide and remain so at all reaction conditions. Pd/PdO thermodynamic data [33,34] show PdO is the stable bulk phase above 10^{-6} kPa O_2 at 623 K and at all conditions used in this study (573–673 K, 10^{-3}–10^{1} kPa O_2^{ν}; PdO favored above 10^{-5} kPa O_2 at 673 K). These thermodynamic data are applicable to bulk structures, in which Pd atoms are predominantly present in the coordinatively saturated environment of a bulk solid. Pd atoms at coordinatively unsaturated corner and edge sites in small clusters tend to oxidize more readily than Pd atoms in larger clusters. Thus, we conclude that the small Pd clusters used here for NO oxidation would also be present as oxides during catalysis.

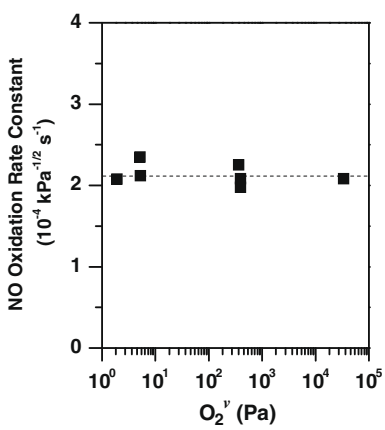

Fig. 5. The forward NO oxidation rate constant ($k_1K_O^{-1/2}$) measured versus oxygen virtual pressure, O_2^{ν}, at 623 K on Pd/Al_2O_3 (0.12 dispersion).

The similar rate expression for metal (Pt [13,14]) and oxide (PdO) catalysts suggests that the oxidation state of the catalyst is inconsequential to the identity of the kinetically relevant elementary steps, although the rate constants for these steps clearly differ among the various catalytic elements.

NO oxidation and oxygen exchange rate constants on Pt catalysts increased markedly with cluster size [14,15]. Similar effects are observed for NO oxidation (Fig. 6a) and oxygen exchange (Fig. 2) rate constants ($k_1K_O^{-1/2}$) on Pd-based catalysts. NO oxidation turnover rate constants increased sharply with increasing PdO cluster size (1–5 nm) and more modestly for clusters above 6 nm. Similar size effects have been reported for CH_4 and dimethylether oxidation on Pd (Fig. 6b) and Pt [30,31,36–38] reactions that also require vacancies on surfaces nearly saturated with O^* or OH^*. These trends reflect larger values of K_O (in Eq. (8)) and smaller concentrations of vacant sites, as a result of the stronger binding of oxygen and hydroxyl species on smaller clusters. O_2 activation rate constants (k_1) may also be affected by cluster size, but they contribute less to the apparent rate constant than K_O because heats of O^* adsorption are much larger than O_2 dissociation barriers on vacant sites [26,39]. Larger metal clusters expose more low-index surface planes, which bind O^* more weakly than the corner and edge sites prevalent on smaller clusters [40,41]. In contrast to Pt, Pd clusters are present as oxides during NO oxidation catalysis. Such PdO clusters are semiconductors [42] for which electron delocalization and small HOMO–LUMO or band gaps are critical for the stability of reduced centers [43,44]. Band gaps vary sensitively with cluster size and increase as domains become smaller and valence electrons become more confined [45]. As a result, vacancies in small oxide clusters are less stable than vacancies in larger clusters because the electrons remaining after oxygen removal must be delocalized into higher energy states [43,44]. Thus, small oxide clusters bind oxygen more strongly than larger clusters [43,44], and oxidation rates that depend on the generation of vacant surface sites are lower on these small clusters [30,31,36–38].

3.5. Effects of NO_2 scavenging on NO oxidation rates

NO_2 inhibits NO oxidation (Eq. (4)) because of its role in determining the concentration of the vacancies required for O_2 activation (Scheme 1, Step 2). Adsorbents can scavenge NO_2 molecules [46] with significant consequences for NO oxidation turnover rates that are inversely proportional to local NO_2 pressure [14]. We examine next NO oxidation rates in catalyst–adsorbent mixtures to determine the inhibiting effects of NO_2 at the low pressures

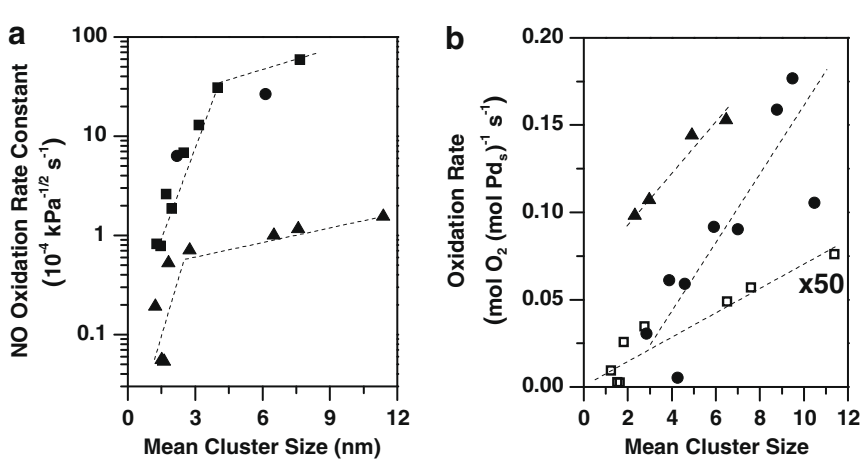

Fig. 6. (a) NO oxidation rate constants ($k_1K_O^{-1/2}$; 603 K) versus cluster size on Pd/Al_2O_3 (▲) and Pt/Al_2O_3 from [14] (■) and [15] (●). (b) Rates of NO oxidation (603 K, □); CH_4 oxidation (553 K, ●) [30]; and dimethylether oxidation (473 K, ▲) [31].

present in NO_x trapping systems and also the effect of catalyst–adsorbent proximity on local NO_2 concentrations.

NO oxidation rates were measured on catalyst pellets with mean radii of 77 and 125 μm that were mixed with adsorbent pellets of the same size, which showed no reactivity toward NO/O_2 mixtures. The resulting NO oxidation and NO_2 elution rates at initial contact times are shown in Table 2. NO consumption rates (0.038–0.046 mol NO $(\text{mol Pd}_s)^{-1}\,\text{s}^{-1}$) were much higher than NO_2 elution rates from the reactor (<0.001 mol NO_2 $(\text{mol Pd}_s)^{-1}\,\text{s}^{-1}$) at these early contact times confirming that adsorbents effectively retained NO_2, which was not detected in the outlet stream. The low NO_2 concentrations were coincident with initial NO oxidation rates that were ~10 times higher than their steady-state value (0.005 mol NO $(\text{mol Pd}_s)^{-1}\,\text{s}^{-1}$), which was reached after ~3 ks when NO_2 pressures were 4 Pa. Initial NO oxidation rates were slightly higher when the pellet size in the reactor decreased from 125 to 77 μm. A substantial decrease in the distance between NO oxidation and NO_2 adsorption sites from mixtures of pellets (77 μm) to mixtures within pellets (<22 μm) led to a relatively modest increase in NO consumption rates (from 0.046 to 0.079 mol NO $(\text{mol Pd}_s)^{-1}\,\text{s}^{-1}$). These data suggest that NO_2 diffusion over distances of ~100 μm weakly influences local NO_2 concentrations, which still inhibit NO oxidation and cause lower rates in the less intimate mixtures. Intrinsic NO_2 adsorption rates, rather than mass transport parameters, affect local NO_2 concentrations in intrapellet and co-impregnated mixtures in NO_x trapping systems.

The absence of mass transfer artifacts in intrapellet mixtures implies that NO_2 can be treated as a reaction intermediate at pseudo-steady-state within intrapellet catalyst–adsorbent mixtures. NO_2 concentrations are then given by the balance between NO oxidation (r_{Pd}) and NO_2 adsorption rates (r_{Ba}):

$$0 = L_{Pd} r_{Pd} - L_{Ba} r_{Ba} \tag{23}$$

Here, L_{Pd} and L_{Ba} represent the number of catalyst and adsorbent sites, respectively. Eq. (23) shows that NO_2 concentrations depend on the relative number of catalyst and adsorbent sites (χ)

$$\chi = L_{Pd}/L_{Ba} \tag{24}$$

Fig. 7 shows the effects of χ, varied by changing the amount of catalyst and adsorbent in intrapellet mixtures, on NO oxidation rates at initial contact times. Initial NO oxidation rates were proportional to $\chi^{-1/2}$ (dashed line). These effects are consistent with an adsorption rate expression that is first order in NO_2:

$$r_{Ba} = k_{Ba}[NO_2] \tag{25}$$

where k_{Ba} is constant for given inlet pressures and temperature. The combination of Eqs. (4) and (23)–(25) leads to an expression for NO_2 concentrations and observed NO oxidation rates in terms of χ, consistent with the results in Fig. 7:

$$[NO_2] = \chi^{1/2}\left(\frac{k_{Pd}[NO][O_2]}{k_{Ba}}\right)^{1/2} \tag{26}$$

$$r_{Pd} = \chi^{-1/2}(k_{Pd}k_{Ba}[NO][O_2])^{1/2} \tag{27}$$

The beneficial effects of decreasing χ on NO oxidation rates imply that the presence of more adsorption sites relative to catalyst sites results in lower NO_2 concentrations. Such low NO_2 concentrations still inhibit NO oxidation via the rate expression in Eq. (5) and the elementary steps in Scheme 1, consistent with the rapid dissociation of NO_2 on catalyst surfaces [39] and with the scarcity of vacancies that facilitate O_2 dissociation. Initial NO oxidation rates correspond to NO_2 pressures and O_2^{ν} between 0.04–0.2 Pa and 10^{-5}–10^{-4} Pa, respectively, as determined by Eqs. (4) and (6) and the measured NO oxidation rate constant. These oxygen chemical potentials remain in the range where PdO is favored over Pd, which undergoes a phase transition at 5×10^{-6} Pa $O_2^{(\nu)}$ at 573 K [33,34]. Catalyst surfaces remain nearly saturated with chemisorbed O^* as a result of strong oxygen adsorption heats (220 and 330 kJ $(\text{mol O}_2)^{-1}$ on Pd clusters of 1 and 3 nm, respectively [47]), which remain relevant to the design of NO_x trapping systems so long as NO_2 binding on adsorbents occurs with finite rates.

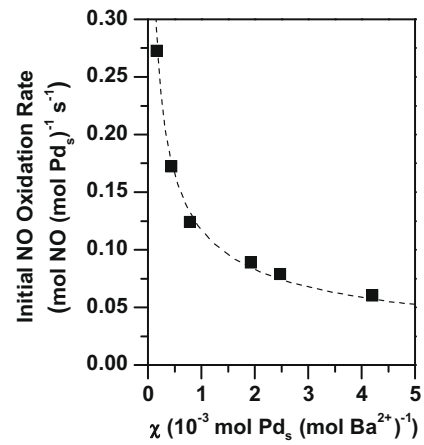

Fig. 7. NO oxidation rates on intrapellet mixtures of Pd/Al_2O_3 (0.12 dispersion) and $BaCO_3/Al_2O_3$ as a function of χ (Eq. (24)) at the initial contact time with 0.18 kPa NO and 1 kPa O_2 at 573 K.

Table 2
NO oxidation rates in catalyst–adsorbent mixtures.

Mean PdO–$BaCO_3$ distance (μm)	Initial NO oxidation rate (mol NO $(\text{mol PdO})^{-1}\,\text{s}^{-1}$)[a]	Initial NO_2 elution rate (mol NO_2 $(\text{mol PdO})^{-1}\,\text{s}^{-1}$)[a]	Initial NO_2 (Pa)	Steady-state NO oxidation rate (mol NO $(\text{mol PdO})^{-1}\,\text{s}^{-1}$)[a]
<22[b]	0.079	<0.001	0.2	0.005
77[c]	0.046	<0.001	0.3	0.005
125[c]	0.038	<0.001	0.4	0.005

[a] Rates measured at 573 K, 0.18 kPa NO, 1 kPa O_2 on mixtures of 10 mg Pd/Al_2O_3 (0.12 dispersion), 125 mg $BaCO_3/Al_2O_3$.
[b] Catalyst and adsorbent combined within pellets from particles sieved to <22 μm.
[c] Catalyst and adsorbent combined as mixtures of pellets with specified mean radii.

4. Conclusions

Kinetic and isotopic measurements led to a consistent mechanistic picture of NO oxidation on PdO clusters involving the kinetically relevant activation of O_2 on isolated vacancies within nearly saturated oxygen adlayers. Vacancy concentrations are diminished in the presence of H_2O, which forms unreactive hydroxyl groups. The O_2 activation steps and their reversibility were confirmed by measurements of oxygen isotopic exchange rates, which were equal to NO oxidation rates at a given value of the oxygen chemical potential. These measurements also showed that the mobility of surface oxygen intermediates allows kinetically relevant dissociation steps to occur on isolated vacancies. NO oxidation turnover rates are insensitive to oxidative or reductive pre-treatments because PdO is thermodynamically favored and forms rapidly at all relevant NO oxidation conditions. NO oxidation rates are instead sensitive to PdO cluster size because oxygen binding energies are higher on small clusters leading to lower vacancy concentrations and turnover rates, a trend that is generally observed for other oxidation reactions that require vacancies on oxygen covered sur-

faces. The requirement for vacancies on PdO surfaces leads to NO_2 inhibition and to significantly higher NO oxidation rates when $BaCO_3$ sites that irreversibly bind NO_2 are present near catalyst sites in physical mixtures.

Acknowledgments

We thank the Ford Motor Company and General Motors for funding. B.W. also acknowledges the Chevron Corporation for a Berkeley–Chevron Fellowship.

References

[1] M.V. Twigg, Appl. Catal. B – Environ. 70 (2007) 2.
[2] N. Takahashi, H. Shinjoh, T. Iijima, T. Suzuki, K. Yamazaki, K. Yokota, H. Suzuki, N. Miyoshi, S. Matsumoto, T. Tanizawa, S. Tateishi, K. Kasahara, Catal. Today 27 (1996) 63.
[3] B.R. Stanmore, J.F. Brilhac, P. Gilot, Carbon 39 (2001) 2247.
[4] S. Salasc, M. Skoglund, E. Fridell, Appl. Catal. B – Environ. 36 (2002) 145.
[5] Y. Su, K.S. Kabin, M.P. Harold, M.D. Amiridis, Appl. Catal. B – Environ. 71 (2007) 207.
[6] H. Shinjoh, N. Takahashi, K. Yokota, Top. Catal. 42 (2007) 215.
[7] B.A. Silletti, R.T. Adams, S.M. Sigmon, A. Nikolopoulos, J.J. Spivey, H.H. Lamb, Catal. Today 114 (2006) 64.
[8] M.M. Yung, E.M. Holmgreen, U.S. Ozkan, J. Catal. 246 (2007) 356.
[9] R. Vijay, R.J. Hendershot, S.M. Rivera-Jimenez, W.B. Rogers, B.J. Feist, C.M. Snively, J. Lauterbach, Catal. Commun. 6 (2005) 167.
[10] A. Amberntsson, E. Fridell, M. Skoglund, Appl. Catal. B – Environ. 46 (2003) 429.
[11] L.D. Li, L.L. Qu, J. Cheng, J.J. Li, Z.P. Hao, Appl. Catal. B – Environ. 88 (2009) 224.
[12] S. Roy, A. Baiker, Chem. Rev. 109 (2009) 4054.
[13] S.S. Mulla, N. Chen, W.N. Delgass, F.H. Ribeiro, Catal. Lett. 100 (2005) 267.
[14] B.M. Weiss, E. Iglesia, J. Phys. Chem. C 113 (2009) 13331.
[15] S.S. Mulla, N. Chen, L. Cumaranatunge, G.E. Blau, D.Y. Zemlyanov, W.N. Delgass, W.S. Epling, F.H. Ribeiro, J. Catal. 241 (2006) 389.
[16] J.E. Benson, H.S. Hwang, M. Boudart, J. Catal. 30 (1973) 146.
[17] D.R. Lide (Ed.), CRC Handbook of Chemistry and Physics, 89th ed., CRC Press, Boca Raton, 2009.
[18] R.M. Koros, E.J. Nowak, Chem. Eng. Sci. 22 (1967) 470.
[19] G. Ketteler, D.F. Ogletree, H. Bluhm, H.J. Liu, E.L.D. Hebenstreit, M. Salmeron, J. Am. Chem. Soc. 127 (2005) 18269.
[20] T. Schalow, B. Brandt, M. Laurin, S. Schauermann, S. Guilmond, H. Kuhlenbeck, J. Libuda, H.J. Freund, Surf. Sci. 600 (2006) 2528.
[21] W.L. Holstein, M. Boudart, J. Phys. Chem. B 101 (1997) 9991.
[22] G.K. Boreskov, Adv. Catal. 15 (1964) 285.
[23] G.K. Boreskov, Discuss. Faraday Soc. 41 (1966) 263.
[24] A. Amirnazmi, J.E. Benson, M. Boudart, J. Catal. 30 (1973) 55.
[25] S.B. Adler, Chem. Rev. 104 (2004) 4791.
[26] A. Eichler, F. Mittendorfer, J. Hafner, Phys. Rev. B 62 (2000) 4744.
[27] A.C. Luntz, J. Grimblot, D.E. Fowler, Phys. Rev. B 39 (1989) 12903.
[28] A.D. Smeltz, R.B. Getman, W.F. Schneider, F.H. Ribeiro, Catal. Today 136 (2008) 84.
[29] J. Au-Yeung, A.T. Bell, E. Iglesia, J. Catal. 185 (1999) 213.
[30] K. Fujimoto, F.H. Ribeiro, M. Avalos-Borja, E. Iglesia, J. Catal. 179 (1998) 431.
[31] A. Ishikawa, E. Iglesia, J. Catal. 252 (2007) 49.
[32] S.S. Mulla, N. Chen, L. Cumaranatunge, W.N. Delgass, W.S. Epling, F.H. Ribeiro, Catal. Today 114 (2006) 57.
[33] J. Nell, H.St.C. O'Neill, Geochim. Cosmochim. Acta 60 (1996) 2487.
[34] W.E. Bell, R.E. Inyard, M. Tagami, J. Phys. Chem. 70 (1966) 3735.
[35] J.Y. Han, D.Y. Zemlyanov, F.H. Ribeiro, Surf. Sci. 600 (2006) 2752.
[36] A. Ishikawa, M. Neurock, E. Iglesia, J. Am. Chem. Soc. 13 (2007) 3048.
[37] R.F. Hicks, H. Qi, M.L. Young, R.G. Lee, J. Catal. 122 (1990) 280.
[38] P. Briot, A. Auroux, D. Jones, M. Primet, Appl. Catal. 59 (1990) 141.
[39] R.B. Getman, W.F. Schneider, A.D. Smeltz, W.N. Delgass, F.H. Ribeiro, Phys. Rev. Lett. 102 (2009) 076101.
[40] R. van Hardeveld, F. Hartog, Surf. Sci. 15 (1969) 189.
[41] B.C. Han, C.R. Miranda, G. Ceder, Phys. Rev. B 77 (2008) 075410.
[42] E. Rey, M.R. Kamal, R.B. Miles, B.S.H. Royce, J. Mater. Sci. 13 (1978) 812.
[43] D.G. Barton, M. Shtein, R.D. Wilson, S.L. Soled, E. Iglesia, J. Phys. Chem. B 103 (1999) 630.
[44] M.D. Argyle, K. Chen, A.T. Bell, E. Iglesia, J. Catal. 208 (2002) 139.
[45] L. Brus, J. Phys. Chem. 90 (1986) 2555.
[46] N.W. Cant, M.J. Patterson, Catal. Today 73 (2002) 271.
[47] P. Chou, M.A. Vannice, J. Catal. 105 (1987) 342.